

SCLoRa: Leveraging Multi-Dimensionality in Decoding Collided LoRa Transmissions

Bin Hu^{†*} Zhimeng Yin^{§*} Shuai Wang^{†‡} Shuai Wang[¶] Zhuqing Xu[†] Tian He[†]

[†] Southeast University, [§]University of Minnesota, [¶]George Mason University
{binhu, shuaiwang, zqxu, tianhe}@seu.edu.cn, yinxx283@umn.edu, swang42@gmu.edu

Abstract—LoRa as a representative of Low-Power Wide Area Networks (LPWAN) technologies has emerged as an attractive communication platform for the Internet of Things. Since its dense deployment, signal collisions at base stations caused by concurrent transmissions degrade network performance. Existing approaches utilize the signal feature, e.g., frequency, to separate packets from collisions. They do not work well in burst traffic networks because the feature is not stable or fine-grained enough and the information for directed signal separation is not sufficient. In this paper, we leverage multidimensional information and propose a novel PHY layer approach called SCLoRa to decode collided LoRa transmissions. SCLoRa utilizes cumulative spectral coefficient, which integrates both frequency and power information, to separate symbols in the overlapped signal. The practical factors of channel fading, similar symbol boundary, and spectrum leakage are taken into account. The SCLoRa design requires neither hardware nor firmware changes in commodity devices – a feature allowing fast deployment on LoRa base stations. We implement and evaluate SCLoRa on USRP B210 base stations and commodity LoRa devices (i.e., SX1278). The experiment results in different scenarios with different radio parameters show that the throughput of SCLoRa is 3× than the state-of-the-art.

I. INTRODUCTION

The Low-Power Wide Area Networks (LPWAN) technologies, including LoRa [1], NB-IoT [2], Sigfox [3] and Weightless [4], have been emerging as popular technologies in recent years [5]. Many LPWAN-based applications, such as Sailing Monitoring System [6], health and well-being monitoring [7], [8], agriculture monitoring [9]–[12], are developed. Since LoRa is designed to support these applications over a long range (e.g., more than 10 KM), a large number of LoRa end devices inevitably coexist at the same time, leading to serious packet loss when these end devices send packets to a base station concurrently [13]. This coexistence has been identified as one of the key challenges [14], which will be more and more critical given the rapid deployment and inevitable burst LoRa traffic.

To ameliorate the problem of LoRa concurrent transmissions, existing approaches are divided into two categories, i.e., MAC-layer approaches and PHY-layer approaches. The MAC-layer approaches address collision issues through collision detection and transmission scheduling. Although these

approaches improve the throughput and reliability of LPWAN, the limited power budget and low cost of LoRa nodes make it challenging to deploy sophisticated MAC methods [15]–[17]. Existing PHY-layer approaches elaborately analyze PHY-level features, such as hardware frequency offset [15] and frequency change [18], that are unique across different LoRa nodes. Admittedly, these techniques have the capability to decouple and demodulate collided concurrent transmissions. They are limited in resolving collisions in large scale LoRa networks since they rely on single LoRa feature which is not fine-grained enough for signal separation of bursty LoRa transmissions.

To support bursty LoRa in the explosive IoT era, we introduce SCLoRa, which utilizes multiple LoRa features at the same time to separate concurrent uplink transmissions. Specifically, we observe that cumulative spectral coefficient, determined by the frequency and power, are unique and reliable across different LoRa devices. This motivates us to distinguish collided LoRa transmissions for demodulation. Although the idea is straightforward, it is a nontrivial task in practice. SCLoRa needs to address several challenges to realize its idea. The first is the dynamic channel fading, leading to volatile spectral coefficients. The second is the similar symbol boundary due to bursty traffic. As a result, we cumulatively evaluate spectral coefficients at different time to increase the reliability and differentiability. To grasp SCLoRa more intuitively, table I shows its comparison with existing methods.

In order to separate packets from overlapped signals, SCLoRa performs the following key steps. First, by analyzing symbols in the window after Fourier transform, the preamble of each signal in the overlapped signal could be detected according to the consecutive symbols. Then we utilize the frequency offset of the upchirp to synchronize the signal, and correct the spectral coefficient of the upchirp as a reference for symbol separation. Finally, we slide the window left and right for each packet and calculate cumulative spectral coefficient of symbols in the window. Each symbol is evaluated by comparing the difference of its cumulative spectral coefficient between actual value and theoretical value. The target symbol for one packet is extracted with the smallest error in cumulative spectral coefficient. We perform this process to estimate the feature for each symbol and each packet respectively and then match the symbols to packets based on the estimation.

*Both authors contributed equally to this work. †Shuai Wang is the corresponding author.

	Features for Signal Separation	Dimensionality for Symbol Classification	Impacts of SNR on performance	Impacts of radio parameters on performance	Demands on Signal Boundary	Adaptability to Burst Traffic
Choir	Frequency Offset	One: Frequency	Medium	Little	No	No
FTrack	Signal Boundary	One: Frequency	Medium	Medium	Yes	No
SCLoRa	Cumulative Spectrum Coefficient	Two: Frequency and Power	Little	Little	No	Yes

TABLE I
COMPARISON OF SCLoRa AND EXISTING SOLUTIONS

The contributions of SCLoRa are summarized as follows

- SCLoRa is the first to examine multiple unique features, e.g., **amplitude** and frequency **offset**, for distinguishing concurrent LoRa packets, in contrast to previous literature that rely on a single feature. This enables SCLoRa to work well in **dense** networks with **bursty** traffic.
- To be resilient to the dynamic environment, SCLoRa introduces cumulative spectral coefficient, which are **determined** by the unique amplitude and frequency offset and also unique across LoRa nodes. In addition, the **challenges** of decoding collided concurrent transmissions with similar symbol boundary and spectrum leakage are addressed.
- We evaluate SCLoRa with USRP and commodity LoRa SX1278 radios. Experiments across different settings demonstrate the effectiveness of SCLoRa, achieving a 3× network throughput of the state-of-the-art.

II. BACKGROUND AND MOTIVATION

In this section, we first introduce how LoRa symbols are modulated and demodulated. Then we introduce the phenomenon of collided LoRa transmissions in burst traffic scenarios, followed by the opportunity of decoding them.

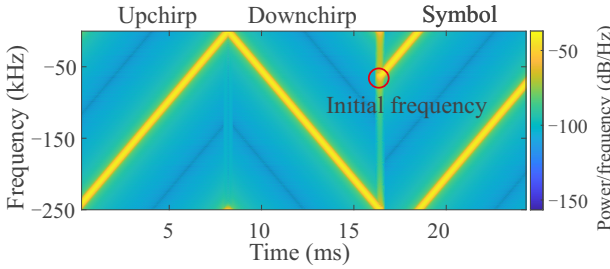


Fig. 1. Signals of the upchirp, the downchirp and the symbol in LoRa.

A. LoRa Modulation and Demodulation

The basic chirp signals in LoRa are the upchirp and the downchirp, as shown in Figure 1. The upchirp/downchirp is a **signal** whose frequency increases/decreases linearly with time. **Modulation:** The frequency of a symbol increases linearly with time. Different symbols are modulated with different **initial** frequencies, as shown in Figure 1. We use $x[n]$ to represent the **signal** sequence of **symbol** p as follows

$$x_p[n] = A_p e^{j2\pi(-f_w + pf_\Delta + nf_\Delta) \frac{n}{N}} \quad (1)$$

where A_p represents signal **amplitude** of symbol p and $-f_w$ represents the lower bound of the symbol frequency. n is the

index of the sequence and N represents the total number of **sampling** points of one symbol. f_Δ is frequency change rate, and $-f_w + pf_\Delta$ represents the **initial** frequency of symbol p . And f_w is the initial frequency of the downchirp with frequency change rate $-f_\Delta$. Then **downchirp** can be expressed as $x_d[n] = A_d e^{j2\pi(f_w - nf_\Delta) \frac{n}{N}}$.

Demodulation: During demodulation, the signal is multiplied by the **standard** downchirp (e.g., $A_d = 1$) as follows

$$\begin{aligned} s_p[n] &= x_{p_s}[n] \times x_d[n] \\ &= A_p e^{j2\pi(-f_w + nf_\Delta + pf_\Delta) \frac{n}{N}} \times e^{j2\pi(f_w - nf_\Delta) \frac{n}{N}} \\ &= A_p e^{j2\pi(pf_\Delta) \frac{n}{N}} \end{aligned} \quad (2)$$

In Equation 2, $s_p[n]$ contains **only** the frequency pf_Δ . Then we perform **FFT** on $s_p[n]$, and we can get the symbol p in the spectrum (e.g., the symbol in Figure 2).

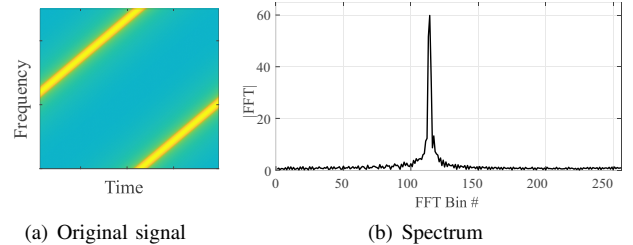


Fig. 2. 2(a) reflects the frequency change of the LoRa symbol over time, and 2(b) is its spectrum after dechirping.

B. Collided Concurrent Transmission

Since LoRa is designed for connecting IoT devices at a long range (e.g., around 10 KM), it is inevitable that there are multiple LoRa **nodes** transmitting at the same time, leading to wireless interference. To tackle this issue, LoRa adopts a technique called spreading factor (SF). Two LoRa transmissions with different SF are **orthogonal** to each other, enabling LoRa receivers to correctly differentiate the target transmission.

As a result, LoRa is able to demodulate LoRa transmissions with different SF parameters, while it fails when there are multiple ongoing LoRa transmissions with **same** SF parameters. This directly limits the communication reliability and network capacity and is more and more critical with the explosive growth of deployed LoRa devices.

To alleviate this issue, recent works, e.g., Choir and FTrack propose to demodulate concurrent LoRa transmissions at the **PHY** layer. By exploiting the unique feature (either frequency offset due to hardware limitation or frequency change), these methods are able to distinguish collided LoRa signals. Although effective, they are still limited by the number of

concurrent LoRa transmissions, since they rely on one single feature of LoRa signal. For example, the hardware frequency offsets could be similar to each other with a large network size in Choir. Similarly, FTrack suffers from inaccurate frequency tracking under similar symbol boundaries, which is more and more likely with an increasing number of LoRa devices. MAC solutions adjust LoRa transmission scheduling to avoid wireless collisions. Although effective, they commonly rely on the knowledge of LoRa traffic requirement, which naturally grows with the network size. As a result, MAC solutions suffer from a performance decrease in a burst traffic scenario. Besides, the MAC solutions and PHY solutions (e.g., SCLoRa) are independent, since they work at different layers. By integrating MAC solutions with PHY solutions, we could further improve LPWAN network reliability and throughput.

C. Opportunities of Decoding Collisions

Motivated by existing literature that rely on a single feature, this work aims to examine multiple LoRa features (e.g., frequency and amplitude) at the same time. This empowers the capability of decoding bursty LoRa concurrent transmissions at a better granularity, which is similar to the well-known problem of classification at higher dimensions. By doing this, we address LoRa collisions and improve the networking capacity, a key issue of current LoRa networks [14]. Although the idea is straightforward, it is challenging to utilize multiple LoRa features in a unified way to reliably decode bursty collided concurrent transmissions under the practical settings including dynamic channel fading and spectrum leakage.

III. DESIGN OF SCLORA

This section analyzes the opportunities of demodulating burst LoRa communication via elaborately utilizing both the frequency and power features of LoRa transmissions. Specifically, Section III-A analyzes the spectral coefficient, which is intrinsically different across LoRa nodes and stable enough within each LoRa transmission, followed by the symbol distinction algorithm that distinguishes concurrent LoRa communication considering both frequency and power difference.

For the illustration purpose, we introduce the calculation of spectral coefficients and symbol classification under the assumption of detected LoRa transmissions, which is achieved through Section III-D. For easy reading, we summarize the key notations used in this paper, as shown in table II.

Symbol	Explanation
$s_p(n)$	It is the signal of the symbol p in the time domain.
$S_p[k]$	It represents the normalized spectral coefficient
Δ_f	It represents the frequency offset.
f_Δ	It is the frequency change rate.
$CSC_p[\Delta_f]$	It represents the cumulative spectral coefficient.
$f_w / -f_w$	It is the upper/lower bound of bandwidth.
$Error_p$	It represents the evaluation result of symbol p .
SC_j	It represents the reference value of spectral coefficient.

TABLE II
SYMBOL SUMMARY

A. Spectral Coefficient

In this section, we first analyze the spectral coefficient of LoRa transmissions in the ideal scenario. With a LoRa symbol p , we denote its signal received at a LoRa receiver as $s_p(n)$. And with dechirping and Fast Fourier transform, we convert the signal to the frequency domain as $S_p[k]$.

$$\begin{aligned} S_p[k] &= \sum_{n=0}^{N-1} s_p(n) e^{-j2\pi \frac{kn}{N}} \\ &= \sum_{n=0}^{N-1} A_p e^{j2\pi (pf_\Delta - k) \frac{n}{N}} \end{aligned} \quad (3)$$

Here N is the total number of sampling points in the window.

Let $\frac{S_p[k]}{N}$ be the spectral coefficients of signal $s_p(n)$, which captures the fundamental harmonics. The spectral coefficient is proportional to $S_p[k]$, so we normalize the spectral coefficient to $S_p[k]$. As Eq.(3) shows, $S_p[k]$ is equal to $\sum_{n=0}^{N-1} A_p$ when k is pf_Δ (i.e., $S_p[pf_\Delta] = \sum_{n=0}^{N-1} A_p$), which is not associated with the specific value of the transmitted symbol p .

In practical scenarios, the symbol boundary is not always aligned with the window boundary, which leads to frequency offset. We set the frequency offset of the symbol as Δ_f , and the time offset of the symbol from the window in the time domain is $\frac{\Delta_f}{f_\Delta}$. Δ_f is determined by the frequency offset of the upchirp in preamble detection duration. And f_Δ is the frequency change rate according to Eq.(1). Because the signal amplitude fluctuates in real-world transmission, we quantify amplitude A_p as $A_p[n] = [A_{p_0}, \dots, A_{p_i}, \dots, A_{p_{N-1}}]$ to easily denote amplitude of each sampling point. As shown in Figure 3(a), due to the frequency offset, only the signal sequence (e.g., the black part) in the window can affect the spectral coefficient. Then the normalized spectral coefficient

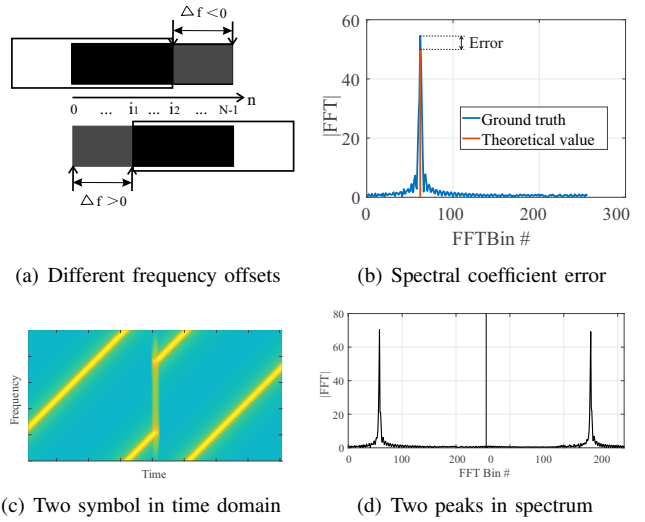


Fig. 3. 3(a) reflects the different boundary offsets. 3(b) shows the error between the ground truth and the theoretical values of the spectrum. 3(c) reflects the frequency change of the LoRa symbol over time, and 3(d) is the spectrum after dechirping.

of the symbol is denoted as follows

$$S_p[pf_\Delta + \Delta_f] = \begin{cases} \sum_{n=-\frac{\Delta_f}{f_\Delta}}^{N-1} A_p[n] & \Delta_f < 0 \\ \sum_{n=0}^{N-1-\frac{\Delta_f}{f_\Delta}} A_p[n] & \Delta_f > 0 \end{cases} \quad (4)$$

From Eq.(4) we find that the spectral coefficient of the symbol is associated with the **power** of the signal and the frequency **offset**. Note that frequency offset is associated with the **time** offset in LoRa.

As shown in the Figure 3(c) and 3(d), two **different** symbols in a packet have the **same** spectral coefficient at their frequency because the **amplitude** of their signal and the **time** offset of each symbol from the window in the time domain are **constant**. SCLoRa utilizes the spectral coefficient to **demodulate** burst LoRa transmissions by examining both **power** and **frequency**.

Since LoRa transmissions are generally **affected** by the varying channel **fading**, the spectral coefficient is volatile in practice. Figure 3(b) depicts the **error** between the theoretical spectral coefficient and the spectral coefficient calculated from the received signal. Figure 4 demonstrates the statistics of the spectral coefficients for different LoRa transmitters. Similar to the theory, the spectral coefficients are generally **stable** within a LoRa transmission and are **different** across distinct LoRa transmitters.

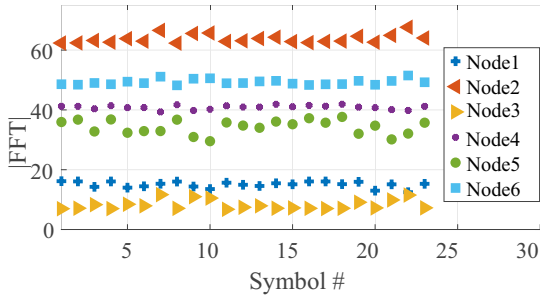


Fig. 4. The Spectral coefficient distribution across LoRa nodes.

Taking the spectral coefficient of Node 3 for example. The normal spectral coefficients are about 12, while the **outliers** of 15 at 7th, 9th, 10th and 22nd symbols also exist, which are very **close** to the spectral coefficients of Node 1. This motivates us to utilize the spectral coefficient in a more sophisticated way, i.e., by considering the spectral coefficient's power and frequency features as discussed in the next section.

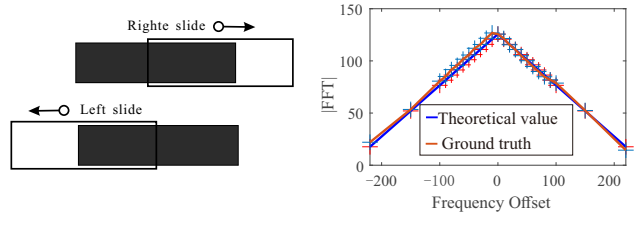
B. Cumulative Spectral Coefficient

To solve the problem of **unstable** spectral coefficients due to the dynamic **fading** and **close** spectral coefficients among symbols, we count the cumulative changes of spectral coefficients over **time**. Since spectral coefficients are related to frequency **offset** and the **amplitude** of the sampling point, when frequency offset changes, the spectral coefficients will change **accordingly**. We define cumulative spectral coefficient as $CSC_p[\Delta_f]$, and the following equation represents the **series** of spectral coefficient, **with** different frequency offsets.

$$CSC_p[\Delta_f] = S_p[pf_\Delta + \Delta_f] \quad , \quad -f_w < \Delta_f < f_w \quad (5)$$

In order to fully describe the change of the symbol's spectral coefficient **with** frequency offset, the **range** of Δ_f ensures the window slide **from** the signal just entering the window **to** completely leaving the window. Importantly, since the frequency of the LoRa signal also changes **linearly** with time, what should be calculated is the spectral coefficient of the **shifted** frequency. After the **symbol** spectral coefficient is **calculated**, the distribution of cumulative spectral coefficient can be obtained by controlling **different** frequency offsets as in Eq.(5).

After the process shown in Figure 5(a), we get the result in Figure 5(b). The blue line is the theoretical value of the cumulative spectral coefficient distribution, and the red line is the ground truth. When the frequency offset is **0**, all sampling points of the symbol are **in** the window. The spectral coefficient reaches the **maximum**. When the frequency offset **increases**, the sampling point of the symbol slides **out** of the window, resulting in a **decrease** in the spectral coefficient. From the results, even if the spectral coefficient calculated at each frequency offset **point** exists an error with the theoretical value, the distribution of the actual cumulative spectral coefficient is very **similar** to the theoretical results. It is clear that **cumulative** spectral coefficient is more **accurate**, compared with a **signal** spectral coefficient.



(a) Sliding window

(b) Cumulative spectral coefficient

Fig. 5. The distribution of cumulative spectral coefficient is obtained through the sliding window.

In addition, cumulative spectral coefficient makes it easier to **distinguish** symbols with similar spectral coefficients. As shown in Figure 6, the target symbol cannot be simply extracted as a result of the **same** spectral coefficients of three **peaks**. When the window slides to the left or right, the **sampling** points of the two **interfering** symbols in the window **increase** accordingly, while the sampling points of the **target** symbol **decrease** in the window. By exploiting this phenomenon, SCLoRa manages to increase the **differences** of **cumulative** spectral coefficient between the interference symbol and the target symbol for **identifying** the target symbol.

Figure 7 depicts the result of **cumulative** spectrum coefficient of the target symbol and the interference. In **particular**, Figure 7(b) reflects the difference of cumulative spectral coefficient of the interfering symbols when the signal boundaries

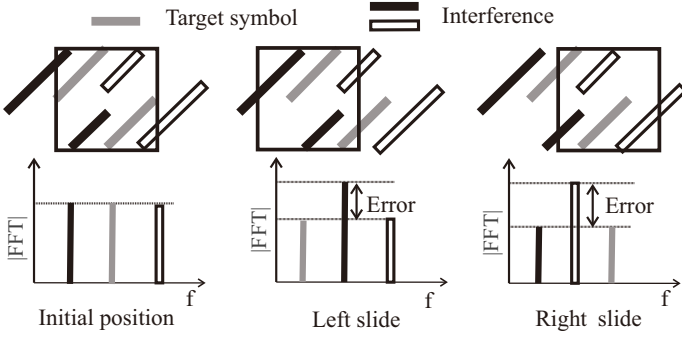


Fig. 6. The window starts with the signal fully aligned and slides left and right, respectively. Left Sliding causes error for symbol in black. And right sliding right causes error for symbol in white.

of the two symbols are aligned. When the boundaries of the signals are close, the power (e.g., A_p) can be used to distinguish the symbols.

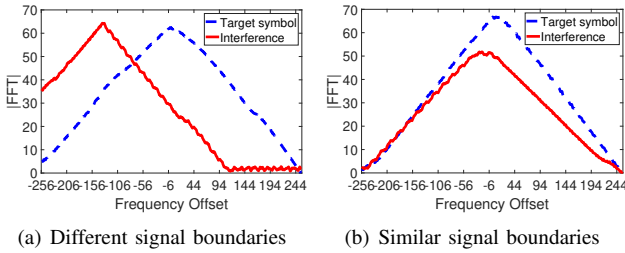


Fig. 7. The cumulative spectrum coefficient distribution of the interfering symbol and the target symbol.

C. Symbol Classification

By calculating cumulative spectral coefficient, we not only reduce the influence of signal amplitude fluctuations but also increase the degree of discrimination between peaks in the window with similar spectral coefficients. Therefore, we use the results of cumulative spectrum coefficient to classify the mixed symbols in the spectrum. Algorithm 1 describes the process of symbol classification.

Algorithm 1 Symbol classification extraction for packet j

```

1: for count=1 to n do
2:    $SC_j = \frac{1}{M} \text{sum}(S_u[k_u]);$ 
3: end for
4: while  $l < \text{PayloadLen}$  do
5:    $s(\text{window}) = x(\text{window}) \times x(\text{downchirp});$ 
6:    $S_p = \text{FFT}(s(\text{window}));$ 
7:   pick( $S_p, p_i$ );
8:   while  $-f_w < \Delta_f < f_w$  do
9:     for  $i=1$  to n do
10:       $Error_i += \text{abs}(SC_j - A_i \frac{\Delta_f}{f_\Delta} - CSC_{p_i}[\Delta_f]);$ 
11:    end for
12:   end while
13:   TargetSymbol=min( $p_i, Error_i$ );
14: end while

```

First, we need to determine the boundary of each signal (described in the next section) and assign a window to each signal. Initially, the boundaries of the allocated windows are respectively aligned with the corresponding signal boundaries, so the spectral coefficient of the target symbol in each window reaches the maximum value for no frequency offset. In order to select the target peak correctly, we evaluate each peak in the initial window. We slide the window according to Eq.(5) and calculate the spectral coefficient of each peak. The evaluation result of each symbol is represented by $Error_p$ as follows

$$Error_p = \sum_{s=-N}^N \left| SC_j - \sum_{i=1}^{|s|} A[i] - CSC_p[sf_\Delta] \right| \quad (6)$$

where $A[i]$ represents the ideal amplitude of the sampling point and each value in it is equal to 1. SC_j is the reference of spectral coefficient(introduced in next section), as a consequence, $SC_j - \sum_{i=1}^{|s|} A[i]$ represents the spectral coefficient of the shifted peak. And $CSC_p[sf_\Delta]$ denotes the actual spectral coefficient of the shifted peak. Since the theoretical value of the spectral coefficient of the target symbol can be calculated, $Error_p$ can be used to represent cumulative spectral coefficient error between the actual value and the theoretical value. After evaluating all the peaks in the initial window, we select the one with the smallest $Error_p$ as the target symbol. Then we align the window with the boundary of the next symbol in the packet and evaluate the peak in the window. Our principle of classifying symbols is to classify the symbols with the smallest evaluation error when the window finishes scanning all the symbols.

D. Packet Processing

This section introduces how SCLoRa detects LoRa transmissions and further demodulates with its spectral coefficients discussed above. To detect ongoing LoRa transmissions, SCLoRa utilizes the preamble detection to identify the LoRa preambles, which are based on the continuously repeated peaks with the same frequency and spectral coefficient in the spectrum. This is effective because even if the time-domain signal is destroyed, the frequency and spectral coefficients in the spectrum can still be effectively extracted. SCLoRa requires a symbol period duration to collect enough samples for distinguishing collided transmissions. This increases to a preamble period when collided signals have aligned boundaries. After identifying LoRa preamble, SCLoRa knows the exact the start of transmission and SF, thus knowing the symbol boundary based on the relationship between frequency offset and time offset. With detected LoRa transmissions, SCLoRa resolves the collision problem of uplink transmission with the following procedures. The basic idea is to go through the packet with cumulative spectral coefficient computation and symbol classification.

To measure the spectral coefficients of different LoRa transmissions, SCLoRa analyzes the preamble signal. When detecting preamble, we calculate the spectral coefficient of each upchirp in the preamble of each signal. We set the

average value of these spectral coefficients in the preamble as a reference value (e.g., SC_j in Algorithm 1) for spectral coefficients of symbols in the payload. We use $S_u[k]$ to represent the spectral components of the upchirp and k_u to represent the frequency of the upchirp in preamble according to Eq.(3). And we count the $Peak(k_u, S_u[k_u])$ of each upchirp in the preamble. We represent the average result of spectral coefficients in the preamble as $\frac{1}{N}SC_j$, which serves as the reference spectral coefficient of each symbol in packet j . And SC_j is defined as follows

$$SC_j = \frac{1}{M} \sum_{i=1}^M S_{u_i}[k_u] \quad (7)$$

where M represents the number of the upchirp in the preamble and u_i represents the upchirp i . In addition to the measurement based on the preamble, SCLoRa also updates the measured spectral coefficients iteratively based on the current LoRa signal, so that it is able to track the dynamic channel.

The overhead of SCLoRa mainly comes from FFT for the calculation of spectral coefficients, which makes the deployment of SCLoRa on programmable base stations feasible. The computation cost of FFT is $O(n \log(n))$. For SCLoRa, to evaluate the symbol by cumulative spectral coefficient, the computation costs of one target symbol extraction becomes $O(n_w N \log(N))$, where N is the number of sampling points in the window and n_w is the number of windows sliding. For the payload length l , the total computation of symbol classification is $O(l n_w N \log(N))$.

E. Spectrum Leakage Elimination

Due to the limited sliding window, the FFT results of LoRa signal suffer from spectrum leakage. To alleviate this issue, we utilize different window functions. Specifically, rectangular window makes the main lobe narrow and the side lobe drop slowly, so the frequency can be more accurate. Blackman window makes the main lobe wider and the side lobe drop quickly, which helps to get the spectral coefficient accurately. The Blackman window makes it easier for us to determine the symbol and the rectangular windows reduce the error of spectral coefficient estimation. We filter the original information by adding Windows twice to make the frequency and spectral coefficient more accurately. In addition, the target frequency is convex in the spectrum, so the frequency identification error can be reduced by setting the part of the spectrum of the non-convex frequency to 0. By doing this, we can effectively reduce the error caused by spectrum leakage.

IV. PERFORMANCE EVALUATION

In this section, we present the experiment results under different settings and the comparison with existing methods. We implement SCLoRa and perform experimental evaluations at USRP B210 and LoRa commodity nodes, which are shown at Figure 8. The commodity nodes use the STM32 chip as the main control chip, SX1278 as the radio frequency chip, and the 3.7v lithium battery to power the entire equipment. The crystal oscillator circuit that provides the clock for the master

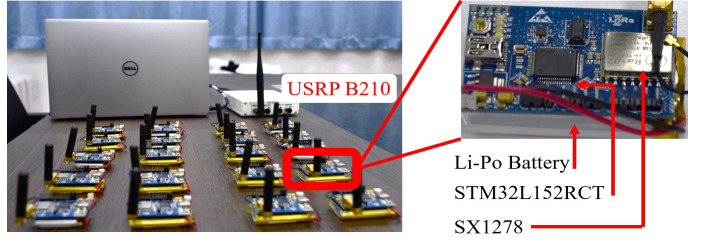


Fig. 8. The scenes of experiments we conducted indoors and the distribution of our equipment. The left part contains 20 SX1278 commodity nodes, a USRP B210, and a laptop. The right part depicts some detailed distributions on commodity nodes, in which STM32L152RCT, SX1278 and Li-Po batteries are used.

chip adopts the ST recommended routing method to minimize the interference of the environment and electromagnetic. And we also used MATLAB for signal processing. Both our USRP B210 and commodity nodes operate at 510MHz bands. In our experiments, we use commodity nodes as the sender to transmit data, and then we use USRP B210 as the base station to receive signals transmitted by the commodity nodes. The USRP B210 is connected to a Dell XPS13 and is controlled by Gnu-Radio.

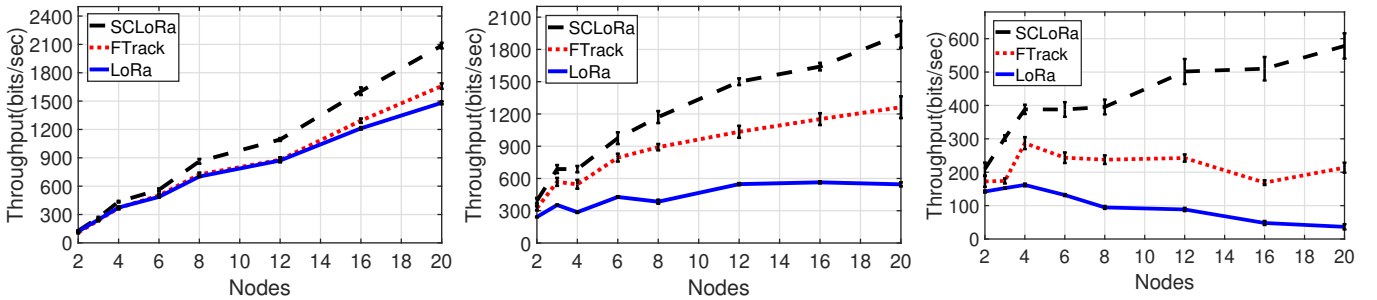
Our experiments are conducted on a university campus. Indoor experiments are conducted in an experimental building, while outdoor experiments are conducted on playgrounds and on campus roads. There is nearly no equipment working in the 510MHz band in our experimental environment, so we can more easily control our settings and environment. Our commercial equipment supports a variety of SF and bandwidth, mainly including SF6 to SF12 and bandwidths of 62.5KHz, 125KHz, 250KHz, 500KHz.

Next, we will evaluate the performance of SCLoRa in different environments and different RF parameter settings. In the experiments, we mainly compare SCLoRa with the two technologies FTrack [18] (e.g., the-state-of-art) and LoRa [1] (i.e., the actual LoRa).

A. Main performance

a) Performance of different numbers of nodes: To explore the impact of the number of nodes in the network on the performance, we conduct the following experiments. In the experiments, the number of nodes is from 2 to 20, and the bandwidth of all nodes is 125KHz. Figure 9 shows the results when the SF is 8, 10, and 12, respectively. The packet sending interval is random (i.e., 1000-2200ms). The packet contains a 22-byte payload and 8 upchirps preamble.

As shown in Figure 9, we evaluate SCLoRa by analyzing the throughput of the network. In the three figures, the collision is most serious at SF12, followed by SF10 and SF8. The result shows that FTrack does not perform well when the SF is small. Because when SF becomes smaller, the symbol duration becomes shorter. When the signals collide, a shorter duration results in similar signal boundaries. For FTrack, similar signals boundaries will cause collided signals to be indistinguishable. In addition, the large SF causes the symbol duration to be



(a) Throughput of different network scale at SF8 (b) Throughput of different network scale at SF10 (c) Throughput of different network scale at SF12

Fig. 9. The network throughput varies with the network size under different SF: 9(a) depicts the case when SF is 8, 9(b) depicts the case where SF is 10, and 9(c) depicts the case where SF is 12.

longer, and the channel occupancy will increase significantly. In this case, as shown in Figure 9, even when the number of nodes and the number of transmitted packets increase, severe collisions cause LoRa's throughput to decrease significantly. For FTrack, as the number of nodes increases, the boundaries of more signals are similar, which makes separation difficult.

b) The performance with different SNRs: In this experiment, we explore the performance with different SNR. The experiment is also carried out indoors, where four nodes are used as terminal devices for transmission with the same parameters(bandwidth=125KHz, packet sending interval=(100–200ms), carrier frequency=510MHz). The packet contains a 22-byte payload and 8 upchirps preamble. We conducted comparative experiments in three SF(e.g., SF8, SF10, and SF12) at low SNR(< 5dB), medium SNR(5 – 20dB), and high SNR(> 20dB) as shown in Figure 10.

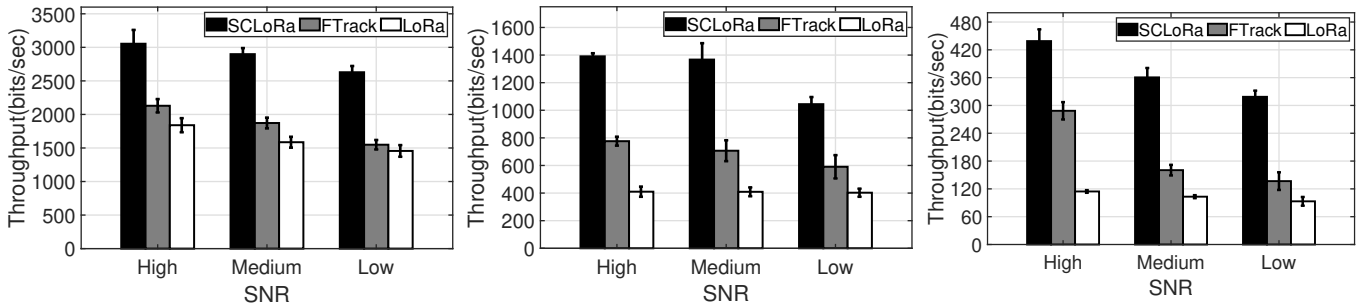
From Figure 9 we can see that SCLoRa has the highest throughput, followed by FTrack, and the lowest is LoRa. And it can be observed that when the SF is small (SF8), the performance of FTrack is similar to LoRa, especially when the SNR is low. When the signals are overlapped, a small SF may make the boundary of signals close, which makes it difficult to distinguish symbols for FTrack. In addition, frequency extraction is not very accurate at low SNR for FTrack, which makes solving collision more difficult. From the experimental results, we can see that SCLoRa is less affected when the SNR decrease. This is because cumulative spectrum coefficient can effectively identify the noise interference.

c) Performance of different duty cycles: We evaluate the performance of SCLoRa under burst traffic. The sudden traffic may be caused by two reasons: dense deployment and expanding packet delivery ratio [19] in the network. In real usage scenarios, low power device LoRa can adopt a duty cycle of 2% [18]. In order to facilitate the evaluation of our experiments, we will increase the duty cycle of the device to simulate burst traffic scenarios. We will compare the performance of the base station to deal with collisions during concurrent transmission at three different duty cycles (duty cycle = 10%, 20%, and 40%). All end devices tested here maintain the same SF=8 and the same bandwidth = 125KHz and center frequency=510MHz. We set up 20 end devices

indoors, and a USRP B210 as a base station to receive their packets. If the devices in the real environment are set with a 2% duty cycle, then three different duty cycles can represent 100, 200, and 400 devices in the network for concurrent transmission.

The results of the experiment are shown in Figure 11(a). We compared the throughput of SCLoRa, FTrack and LoRa. The evaluation results show that SCLoRa performs best, followed by FTrack, and LoRa has the worst performance because it does not have the ability to resolve conflicts. For FTrack, the core of its design is to utilize the different boundaries of conflicting signals to distinguish the signals, and its performance is easily affected by RF parameters (e.g., SF and bandwidth). Here we set a smaller SF, which may lead to certain performance limitations of FTrack. Because shorter symbols lead to shorter air time [20], the signal boundaries are similar or the same, which cannot be solved by FTrack. From Figure 11(a), we can see that the throughput of SCLoRa is much higher than FTrack. For SCLoRa, we utilize the cumulative change error of LoRa symbol spectral coefficients to resolve collisions. The spectral coefficient of the LoRa symbol is related to the boundary of the signal and the amplitude of the sampling point. Therefore, when the signal boundaries are similar, the spectral coefficients of the LoRa symbol may still be different because of the different power of the signal. In the process of cumulatively calculating the spectral coefficient error, the difference between the target symbol and the interfering symbol will also increase, so we can more effectively separate the conflicting signals.

d) The performance of different distance: In order to explore the performance of SCLoRa at different distances, we fix the base station and place LoRa nodes at different locations on the campus to test the throughput. As shown in Figure 12, we place the USRP B210 and the laptop at P1 and four nodes at P2 – P9. The marked points represent the place of the campus road where many buildings and trees on both sides of the road which may affect the signal transmission. The distances of P2-P9 from P1 are shown in Figure 11(b). The bandwidth of these devices is 125KHz and the packets including a payload of 22 bytes and a preamble of 8 upchirps are sent in a small random interval(100–220ms). As



(a) The comparison of three approaches at SF8. (b) The comparison of three approaches at SF10. (c) Comparison of three approaches at SF12.

Fig. 10. The throughput of three approaches (SCLoRa, FTrack, LoRa) with different SNR under different SF (8, 10, 12).

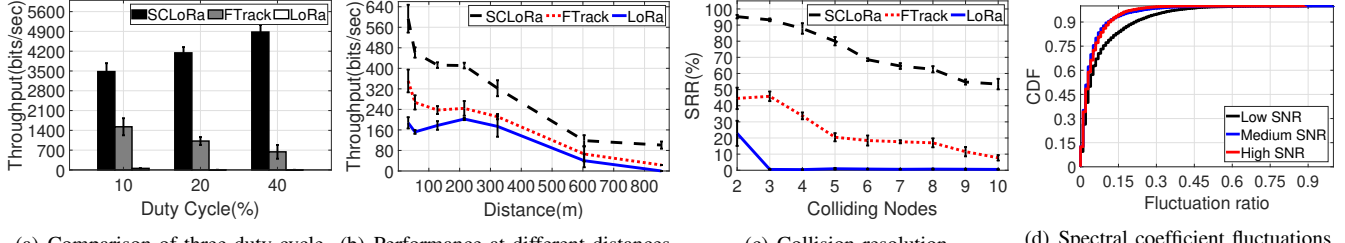


Fig. 11. 11(a) the throughput of three approaches at different duty cycles. 11(b) the performance of concurrent transmission at different distances. 11(c) shows the performance of collision resolution. 11(d) the distribution of the spectral coefficient of the symbols at different SNR.

a result of the hardware limitations and parameter settings, the communication distance of our equipment could reach nearly 1 kilometer.

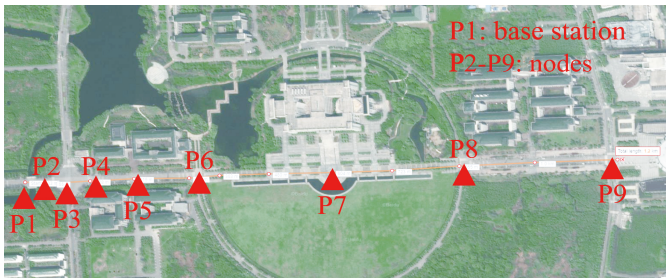


Fig. 12. Outdoor experiment scene: the satellite map of the campus. We place our equipment at points P1-P9 respectively.

From Figure 11(b), we find that as the communication distance increases, the throughput of various approaches decreases. The major drop in the throughput is mainly due to the obvious attenuation of the LoRa signal in the transmission process in the real environment. As the communication distance increases, SCLoRa still guarantees the highest throughput. SCLoRa has a better effect on solving this problem, not only benefit by the CSS modulation technology used by LoRa but also because SCLoRa makes full use of the characteristics of CSS technology by constructing more reliable symbol classification models based on cumulative spectral coefficient.

e) **SRR at different bandwidth:** The factors that affect the performance of LoRa concurrent transmission are not only scene changes but also the parameter settings. So in order to explore this impact of different bandwidths on SCLoRa

performance, we conducted the following experiments. Our experiments are performed in the laboratory. The bandwidth of four nodes and USRP B210 are set as 62.5KHz, 125KHz and 250KHz. The packets including a payload of 22 bytes and a preamble of 8 upchirps are sent in a small random interval(100-220ms).

As the bandwidth becomes larger, the symbol duration becomes shorter, which makes the signal collisions fewer. From Figure 13, it can be observed that as the bandwidth increases, the performance of the three approaches has been improved. In the comparison of the symbol reception rate (SRR) of the three approaches, SCLoRa has the highest SRR, FTrack is second, and LoRa is the lowest. Besides, a small SF results in a small symbol duration and a small channel occupation, so there is less signal collision. As a result, when the SF is stable, as the bandwidth increases, the SRR also becomes larger. The comparison results of SCLoRa, FTrack and LoRa show that SCLoRa is more suitable for concurrent scenarios. Especially when the BW is small and the SF is large, SCLoRa can still keep good performance. This is mainly because the signal boundary does not have a significant impact on SCLoRa(e.g., the spectral coefficient is related to frequency deviation and power).

B. Collision resolution capability

In order to intuitively illustrate SCLoRa's ability to resolve signal collisions during concurrent transmission, we conducted the following experiments. We achieve different degrees of conflict by increasing the number of colliding nodes(from 2 to 10). In order to ensure that all nodes will collide during transmission, we reduce the transmission cycle of all nodes and

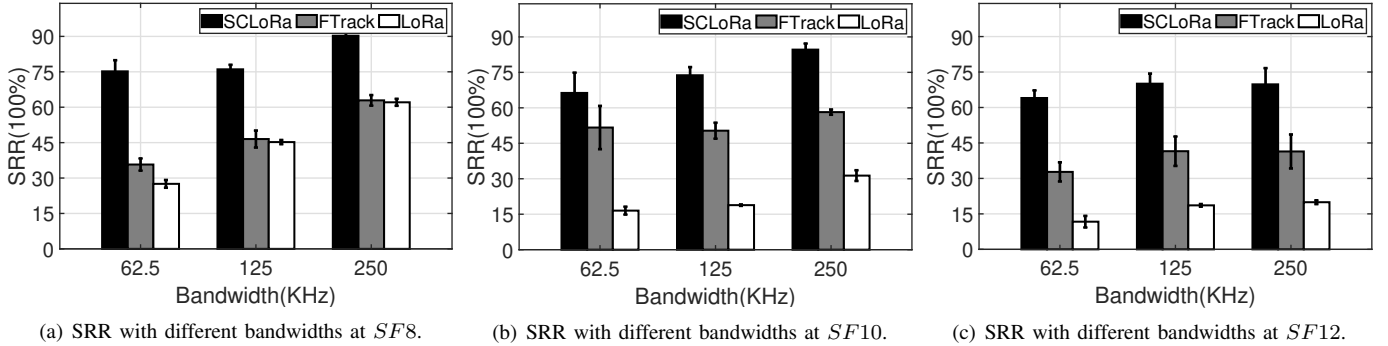


Fig. 13. The symbol reception rate(SRR) of concurrent transmission at different bandwidth.

set their duty **cycle** to be **greater** than 50%. The experiment is conducted in the school's laboratory, during which there is no interference from other signals. We evaluate the ability to resolve collisions by measuring the symbol reception rate (**SRR**) at the base station. And we compare the performance of SCLoRa with FTrack and LoRa.

The experimental results are shown in the Figure 11(c), and the three lines represent the symbol reception rate of three different technologies when a signal collision occurs. We observe that SCLoRa performs best in the ability to resolve signal collisions during concurrent transmission, followed by FTrack, and LoRa performs the worst because it does not have the **ability** to resolve collisions. In this experiment, due to the high **duty cycle** of the transmitted signal, the collision signal **boundary** will be relatively **close**, especially when the number of colliding nodes increases. Since SCLoRa considers the information of frequency offset **and** power in two dimensions, it is easier to distinguish the symbols in the case of such symbol mixing.

C. SCLoRa overhead

Computation overhead: We compare the computation overhead of SCLoRa and FTrack. Table III shows the average overhead of correctly demodulating a LoRa symbol of different numbers of concurrent LoRa transmissions. The computation overhead increases with the total **number** of nodes. On average, SCLoRa's computation overhead is 69.87% lower than that of FTrack.

Energy consumption: We also compare the energy consumption of LoRa nodes in both SCLoRa and FTrack designs. When LoRa packets are corrupted, LoRa nodes are required to **retransmit**, leading to higher energy consumption. Table IV demonstrates the energy consumption of LoRa nodes to successfully transmit one LoRa packet of different **numbers** of concurrent LoRa nodes. Since SCLoRa offers better communication **reliability** under collisions, LoRa nodes manage to save more energy consumption. For example, the energy consumption of SCLoRa is 56.46% lower than that of FTrack when the number of concurrent transmissions equals four.

D. Design insights

a) **Spectral coefficient stability:** In SCLoRa, the spectral coefficient of LoRa signal is mainly used to **classify** symbols.

No. of Collided Trans	2	4	6	8	10
SCLoRa (ms)	0.64	1.61	1.95	2.14	2.36
FTrack (ms)	1.12	3.98	9.11	10.79	20.16

TABLE III
OVERHEAD COMPARISON

No. of Collided Trans	2	4	6	8	10
SCLoRa ($\times 10^{-3} J$)	2.29	2.63	3.17	3.64	4.59
FTrack ($\times 10^{-3} J$)	4.76	6.04	8.77	13.02	19.50

TABLE IV
ENERGY COMPARISON

In order to verify the **reliability** of the theory that the spectral coefficient of symbol remains stable in **one** packet, we evaluate the spectral coefficients of the target symbols in the **packet** in the real environment. We measure the **fluctuation** of the spectral coefficients by measuring the standard **deviation** of a set of symbols in multiple packets. From the previous description, we know that the spectral coefficient is related to the power of the signal **and** the frequency offset of the symbol. **Noise** is likely to affect the spectral coefficient of the symbol because it affects the **power** of the signal. So we measure the fluctuation of the spectral coefficients in the LoRa packet at low SNR($< 5dB$), medium SNR($5-20dB$) and high SNR($> 20dB$) by commodity nodes.

The three **curves** in Figure 11(d) respectively count the CDFs of the **stability** of the spectral coefficients of the symbols at different SNR. In Figure 14, the fluctuation ratio represents the **error** ratio of actual value to the theoretical value. At high and medium SNR, the fluctuation ratio of the spectral coefficient approximately reaches 90% of the symbols. Even at low SNR, the fluctuation rate of the spectral coefficient of approximately reach 80% of the symbols. The above experimental results show that the spectral coefficients of the symbols in a **packet** are almost stable. So it is feasible to use the spectral coefficients of the symbols to distinguish different signals.

b) **Spectral coefficient changes as the window slides:** In SCLoRa, we establish an accurate symbol classification model based on **cumulative** spectral coefficient. To illustrate the **reliability** of the model, we measure the **error** between the actual value of spectral coefficient under the window sliding and the theoretical value. Considering the effect of **noise**, our experiments are performed at low SNR($< 5dB$), medium SNR($5-20dB$) and High SNR($> 20dB$). In addition, in

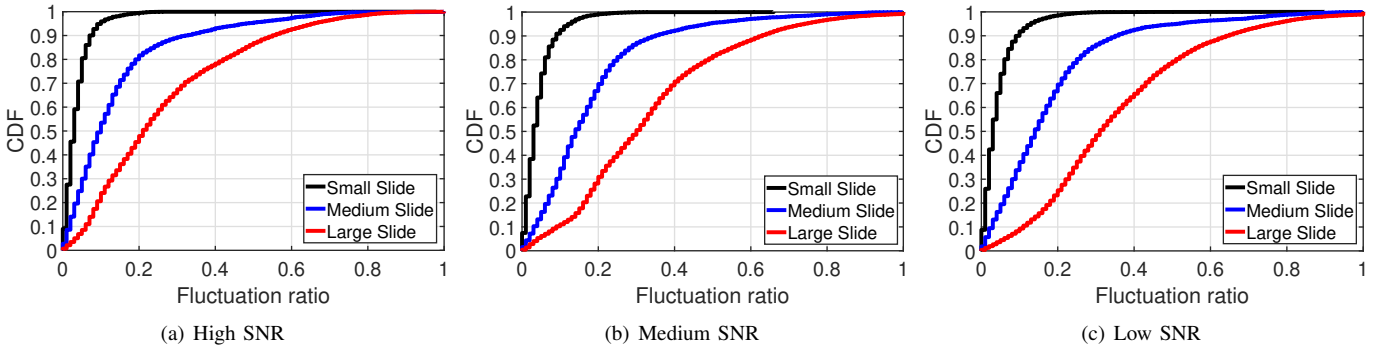


Fig. 14. The fluctuation ratio between the spectral coefficient of the ground truth when the window is sliding.

order to explore the change of the symbol's spectral coefficient under different degrees of window slide, we set small slide($< 1/3$ symbol duration), medium slide($1/3 - 2/3$ symbol duration), and large slide($> 2/3$ symbol duration) respectively for experiments.

In Figure 14, the fluctuation ratio represents error rate of actual value to theoretical value. And we can find that when the window is sliding, the stability of the symbol's spectral coefficients is best at high SNR, then medium SNR, and low SNR at worst. Comparing the small slide, medium slide and large slide, we find the small slide brings the highest stability of the spectral coefficients, almost all less than 0.2, followed by the medium slide (0.4), and the worst is the large slide (0.6). This is because a large slide causes fewer signals of the target symbol in the window, and the spectral coefficient of the target symbol is easily affected by the neighboring symbols and the overlapped symbols. Therefore, when calculating cumulative spectral coefficient, we need consider the weight of sliding Windows to different degrees to ensure more accurate symbol classification results.

V. RELATED WORK

The problem of collision in wireless networks has always been the focus of attention. In fact, as the challenges of LPWAN: capacity and coexistence [14], concurrent transmission becomes an inevitable form, and the resolution of signal collision problems in concurrent transmission becomes more important. There are two types of approaches: MAC approaches and PHY approaches, which are two different levels of solutions and do not conflict but even collaborate with each other. The MAC solution, such as [21]–[24], can guarantee the communication order in the network, thereby maximizing the effective utilization of the network capacity, improving the throughput of the network, and ensuring reliable communication. The PHY solution, such as [15], [18], [25]–[28], extracts valid information after signal collision.

Orthogonal signals can effectively improve the possibility of concurrent transmission, [29], [30] explain the orthogonality between LoRa symbols, which can improve the utilization of the channel. By combining interference management and interference cancellation, the technology overcomes the problem of the throughput limitation in the MIMO LAN [31]. And many solutions use the nature of various wireless technologies to

solve the PHY layer collision problem [15], [25], [32]. [32] uses the constellation diagram to implement parallel decoding for cots RFID tags. [25] uses the relationship between signal points of ZigBee to extract the phase. [15] uses the imperfections of the hardware itself to separate the superimposed LoRa symbols.

The characteristics of LoRa is based on chirp spread spectrum(CSS) modulation. In CSS-based ranging studies, signal collisions are prevented by using backoff time [33]. In recent researches, instead of retransmitting the entire frame, the terminal device continuously transmits the bitmap to determine the correct symbol for each collision frame [34], and full synchronization of the signal is required. For signals that are not synchronized, the proposed algorithm [35] maps the symbols together according to the change of the symbols at different signal boundaries. FTrack [18] separates each symbol by tracking the frequency of chirp, which performs better in cases where the boundaries of the signal are not aligned. Similarly, it is not easy for Choir to distinguish the frequency offset caused by hardware in burst traffic. mLoRa [28] uses sample-by-sample and then chirp-by-chirp to decode conflicting packets, but this method is not applicable to simultaneous collisions of multiple nodes. Compared with prior work, SCLoRa is more suitable for burst LoRa traffic since multidimensional information make it more differentiable for decoding collided concurrent transmissions.

VI. CONCLUSION

In this paper, we propose a novel design called SCLoRa to solve the collision of multiple concurrent LoRa transmissions. SCLoRa makes no hardware or firmware changes in LoRa end devices and is deployable on programmable base stations. The core of our design is to make use of the spectral coefficient of LoRa signal. By leveraging multi-dimensionality in decoding collided LoRa transmissions, SCLoRa further improves the up-link transmissions. The experiment results show that SCLoRa performs well and is suitable for burst traffic scenarios.

ACKNOWLEDGMENT

This work was supported in part by the National Natural Science Foundation of China under Grant No. 6167219, BK20190336, and China National Key RD Program 2018YFB2100302.

REFERENCES

- [1] "Lora alliance." <https://www.lora-alliance.org/>.
- [2] N. Mangalvedhe, R. Ratasuk, and A. Ghosh, "Nb-iot deployment study for low power wide area cellular iot," in *2016 IEEE 27th Annual International Symposium on Personal, Indoor, and Mobile Radio Communications (PIMRC)*, pp. 1–6, IEEE, 2016.
- [3] "Sigfox." <http://www.sigfox.com/en/>.
- [4] "Weightless." <http://www.weightless.org/>.
- [5] R. Sanchez-Iborra and M.-D. Cano, "State of the art in lp-wan solutions for industrial iot services," *Sensors*, vol. 16, no. 5, p. 708, 2016.
- [6] L. Li, J. Ren, and Q. Zhu, "On the application of lora lpwan technology in sailing monitoring system," in *2017 13th Annual Conference on Wireless On-demand Network Systems and Services (WONS)*, pp. 77–80, IEEE, 2017.
- [7] P. A. Catherwood, D. Steele, M. Little, S. Mccomb, and J. McLaughlin, "A community-based iot personalized wireless healthcare solution trial," *IEEE journal of translational engineering in health and medicine*, vol. 6, pp. 1–13, 2018.
- [8] J. Petäjäjärvi, K. Mikhaylov, R. Yasmin, M. Hämäläinen, and J. Iinatti, "Evaluation of lora lpwan technology for indoor remote health and wellbeing monitoring," *International Journal of Wireless Information Networks*, vol. 24, no. 2, pp. 153–165, 2017.
- [9] H. M. Jawad, R. Nordin, S. K. Gharghan, A. M. Jawad, and M. Ismail, "Energy-efficient wireless sensor networks for precision agriculture: A review," *Sensors*, vol. 17, no. 8, p. 1781, 2017.
- [10] S. Benissa, D. Plets, E. Tanghe, J. Trogh, L. Martens, L. Vandaele, L. Verloock, F. Tuytens, B. Sonck, and W. Joseph, "Internet of animals: characterisation of lora sub-ghz off-body wireless channel in dairy barns," *Electronics Letters*, vol. 53, no. 18, pp. 1281–1283, 2017.
- [11] D. Sartori and D. Brunelli, "A smart sensor for precision agriculture powered by microbial fuel cells," in *2016 IEEE Sensors Applications Symposium (SAS)*, pp. 1–6, IEEE, 2016.
- [12] D. Ilie-Ablachim, G. C. Pătru, I.-M. Florea, and D. Rosner, "Monitoring device for culture substrate growth parameters for precision agriculture: Acronym: Monisen," in *2016 15th RoEduNet Conference: Networking in Education and Research*, pp. 1–7, IEEE, 2016.
- [13] J. Haxhibeqiri, F. Van den Abeele, I. Moerman, and J. Hoebeke, "Lora scalability: A simulation model based on interference measurements," *Sensors*, vol. 17, no. 6, p. 1193, 2017.
- [14] B. Ghena, J. Adkins, L. Shangguan, K. Jamieson, P. Levis, and P. Dutta, "Challenge: Unlicensed lpwans are not yet the path to ubiquitous connectivity," in *The 25th Annual International Conference on Mobile Computing and Networking*, pp. 1–12, 2019.
- [15] R. Eletreby, D. Zhang, S. Kumar, and O. Yağan, "Empowering low-power wide area networks in urban settings," in *Proceedings of the Conference of the ACM Special Interest Group on Data Communication*, pp. 309–321, ACM, 2017.
- [16] A.-A. A. Boulogiorgos, P. D. Diamantoulakis, and G. K. Karagiannidis, "Low power wide area networks (lpwans) for internet of things (iot) applications: Research challenges and future trends," *arXiv preprint arXiv:1611.07449*, 2016.
- [17] M. Centenaro, L. Vangelista, A. Zanella, and M. Zorzi, "Long-range communications in unlicensed bands: The rising stars in the iot and smart city scenarios," *IEEE Wireless Communications*, vol. 23, no. 5, pp. 60–67, 2016.
- [18] X. Xia, Y. Zheng, and T. Gu, "Ftrack: parallel decoding for lora transmissions," in *Proceedings of the 17th Conference on Embedded Networked Sensor Systems*, pp. 192–204, 2019.
- [19] K. Vikram and S. K. Sahoo, "A collaborative framework for avoiding interference between zigbee and wifi for effective smart metering applications," *Electronics*, vol. 22, no. 1, pp. 48–56, 2018.
- [20] J. C. Liando, A. Gamage, A. W. Tengoutius, and M. Li, "Known and unknown facts of lora: Experiences from a large-scale measurement study," *ACM Transactions on Sensor Networks (TOSN)*, vol. 15, no. 2, pp. 1–35, 2019.
- [21] Z. Hu and C.-K. Tham, "Ccmac: coordinated cooperative mac for wireless lans," in *Proceedings of the 11th international symposium on Modeling, analysis and simulation of wireless and mobile systems*, pp. 60–69, ACM, 2008.
- [22] M. C. Bor, J. Vidler, and U. Roedig, "Lora for the internet of things.," in *EWSN*, vol. 16, pp. 361–366, 2016.
- [23] B. Reynders, W. Meert, and S. Pollin, "Power and spreading factor control in low power wide area networks," in *2017 IEEE International Conference on Communications (ICC)*, pp. 1–6, IEEE, 2017.
- [24] J.-T. Lim and Y. Han, "Spreading factor allocation for massive connectivity in lora systems," *IEEE Communications Letters*, vol. 22, no. 4, pp. 800–803, 2018.
- [25] L. Kong and X. Liu, "mzig: Enabling multi-packet reception in zigbee," in *Proceedings of the 21st annual international conference on mobile computing and networking*, pp. 552–565, ACM, 2015.
- [26] M. Benbaghdad, B. Fergani, and S. Tedjini, "Toward a new phy layer scheme for decoding tags collision signal in uhf rfid system," *IEEE Communications Letters*, vol. 20, no. 11, pp. 2233–2236, 2016.
- [27] Y. Cao, Z. Wang, L. Kong, G. Chen, J. Yu, S. Tang, and Y. Chen, "Forward the collision decomposition in zigbee," in *2019 IEEE 27th International Conference on Network Protocols (ICNP)*, pp. 1–11, IEEE, 2019.
- [28] X. Wang, L. Kong, L. He, and G. Chen, "mlora: A multi-packet reception protocol in lora networks," in *2019 IEEE 27th International Conference on Network Protocols (ICNP)*, pp. 1–11, IEEE, 2019.
- [29] B. Reynders and S. Pollin, "Chirp spread spectrum as a modulation technique for long range communication," in *2016 Symposium on Communications and Vehicular Technologies (SCVT)*, pp. 1–5, IEEE, 2016.
- [30] D. Croce, M. Guicciardo, S. Mangione, G. Santaromita, and I. Tinnirello, "Impact of lora imperfect orthogonality: Analysis of link-level performance," *IEEE Communications Letters*, vol. 22, no. 4, pp. 796–799, 2018.
- [31] S. Gollakota, S. D. Perli, and D. Katabi, "Interference alignment and cancellation," in *ACM SIGCOMM Computer Communication Review*, vol. 39, pp. 159–170, ACM, 2009.
- [32] J. Ou, M. Li, and Y. Zheng, "Come and be served: Parallel decoding for cots rfid tags," in *Proceedings of the 21st Annual International Conference on Mobile Computing and Networking*, pp. 500–511, ACM, 2015.
- [33] H. Cho and S. W. Kim, "An anti-collision algorithm for localization of multiple chirp-spread-spectrum nodes," *Expert Systems with Applications*, vol. 39, no. 10, pp. 8690–8697, 2012.
- [34] S. Abboud, N. E. Rachkidy, and A. Guitton, "Efficient decoding of synchronized colliding lora signals," *arXiv preprint arXiv:1902.05295*, 2019.
- [35] N. El Rachkidy, A. Guitton, and M. Kaneko, "Decoding superposed lora signals," in *2018 IEEE 43rd Conference on Local Computer Networks (LCN)*, pp. 184–190, IEEE, 2018.